Flow Measurements of Translational-Rotational Nonequilibrium Using Laser-Induced Iodine Fluorescence

Eric Cecil and James C. McDaniel

Department of Mechanical and Aerospace Engineering, University of Virginia, Charlottesville, VA 22903, USA

Abstract. A shock wave impingement flow was studied under low temperature, low density conditions in a hypersonic free-jet wind tunnel. A sharp-edged flat plate was placed at zero incidence in the hypersonic core of a free-jet of nitrogen gas at Mach 12; a right circular cylinder mounted in the middle of the plate projected out normal to the plate surface. The oblique shock produced at the plate leading edge impinged on the detached bow shock wave produced by the cylinder.

The symmetry plane in the flow was studied using a laser sheet-beam probe from a narrow-bandwidth laser source, which induced fluorescence in iodine molecules seeded in the gas. Fluorescence patterns produced by the sheet-beam were recorded by a charge-coupled device camera as the laser frequency was tuned in increments over a range spanning two distinct absorption lines in the iodine spectrum. The fluorescence intensity-versus-laser excitation frequency data recorded at each pixel was least-squares fitted to a nonequilibrium model of the iodine spectrum to estimate local translational and rotational temperature, velocity, and density. Contour plots of these results are presented at a resolution equal to roughly one mean-free-path of the oncoming flow at the plate leading edge. Profile plots of translational and rotational temperature on the plate are presented.

INTRODUCTION

A laser-induced fluorescence (LIF) flow diagnostic technique has been developed to measure translational and rotational gas kinetic temperature and has been applied to study thermal nonequilibrium in a Mach 12 shock wave impingement flow produced in a highly underexpanded free jet wind tunnel [1].

Figure 1 is a schematic of the shock impingement model. A sharp-edged flat plate generates a weak shock that impinges on the bow shock produced by a cylinder extending perpendicular to the plate surface, midway along the plate. In the rarefied conditions of the tests, flow slips at the plate surface and the thickness of shock waves is not negligible. The boundary layer is thick and interacts with the shock layer near the leading edge of the plate. The impingement of the oblique shock upon the cylinder bow shock may produce a small supersonic jet which impinges on the cylinder, based on the classification of shock impingement patterns discussed by Edney [2]. Supersonic flow in the shock layer and boundary layer produce a submerged bow shock on the cylinder. Because of these interesting features, this flow was studied as a test of the LIF measurement technique.

IODINE FLUORESCENCE MEASUREMENT TECHNIQUE

Measurement of the laser-induced fluorescence spectra of molecules in a flowing gas provides quantitative information on the local thermodynamic conditions in the flow [3]. A narrowband laser-induced fluorescence measurement technique has been developed to use nuclear hyperfine components of two transition line groups in the $B \leftrightarrow X$ electronic transition of molecular iodine. This measurement technique was developed to study low temperature supersonic flows of I_2-seeded N_2 gas.

A tunable single frequency laser beam is expanded and collimated into a thin sheet and passed into a low density wind tunnel flow, causing I_2 molecules to fluoresce within a chosen plane of the flow-field. A series of images are taken of the fluorescence with a charge-coupled device (CCD) array as the laser frequency is incrementally tuned over selected lines in the I_2 absorption spectrum. Fluorescence intensity versus frequency data may be extracted from the series of images at any point in the plane of the laser sheet, within the resolution of the digital image.

Measured intensity versus frequency data were fitted to a mathematical model of the iodine spectrum using a non-linear least-squares regression method. The iodine spectrum model relates the spectrum line shape to parameters of interest in the flow such as temperature, density, and (via frequency shift) velocity. For the present investigation,
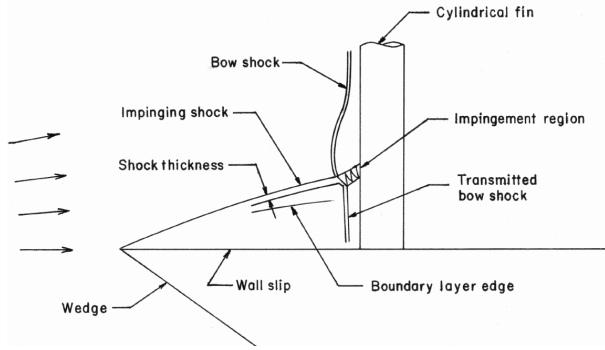
FIGURE 1. Schematic of shock wave interaction model in slip flow regime.
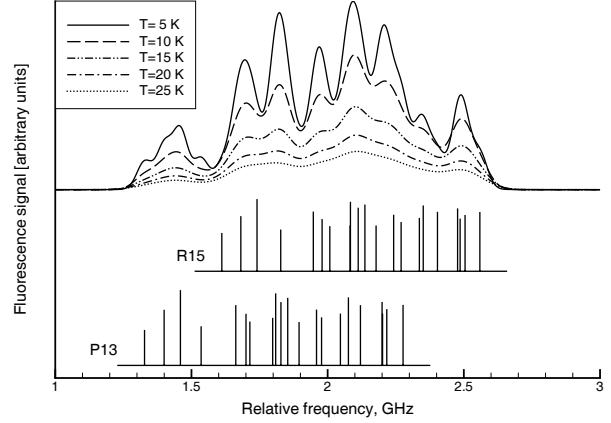
FIGURE 2. Computed P13,R15 hyperfine lineshape at low temperatures, plotted at very low constant pressure.

translational, rotational, and vibrational kinetic temperature were treated as independent fitting parameters controlling translational, rotational, and vibrational energy mode contributions of the iodine molecule to the line shape. (Vibrational temperature was assumed to be "frozen" to a constant value in the free jet expansion.)

The least-squares curve fit model was written

$$S_m = c_1 S_f(T_{tran}, T_{rot}, T_{vib}, n, \nu - \Delta\nu) + c_2(\nu). \tag{1}$$

The scaling factor c_1 was determined by a single curvefit at an upstream point on the jet centerline with known density and temperature, and was retained as a fixed parameter in all subsequent fits. The term $c_2(\nu)$ represents a weak unshifting background spectrum due to fluorescence induced by laser light scattered from the model surface. This source of noise in the data was evaluated at a location not directly illuminated by the laser sheet, and in effect was subtracted from all the flowfield spectra.

The fluorescence signal produced by I_2 vapor (in a low pressure carrier gas at rest) from a single transition line i, centered at frequency $\nu_{0,i}$, due to excitation at frequency ν, is given by
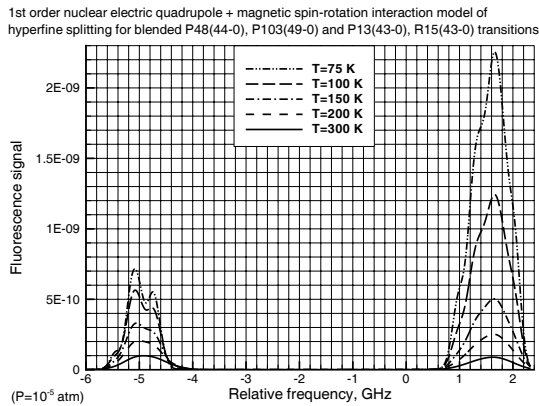
$$S_{f_i}(\nu) = C I n f_{\nu''J''}(T_{rot}, T_{vib}) \, q_{\nu'\nu''} g_{hf} S_{hf,i} \frac{S_{J'J''}}{2J''+1} \frac{V(\nu, \nu_{0,i}, n, T_{tran})}{\Delta\nu_D(T_{tran})}, \tag{2}$$

where C is a constant representing signal collection efficiency and molecular constants, I is excitation source intensity, n is gas number density, T_{tran}, T_{rot}, and T_{vib} are respectively translational, rotational, and vibrational temperature, $f_{\nu''J''}$ is the Boltzmann population of the ground vibrational-rotational state $v'' J''$, $q_{\nu'\nu''}$ is the Franck-Condon factor, g_{hf} is the hyperfine degeneracy, $S_{hf,i}$ is the hyperfine line strength, $S_{J'J''}$ is the Hönl-London rotational line strength, and $\Delta\nu_D(T_{tran})$ is the Doppler line width. The Voigt function $V(\nu, \nu_{0,i}, n, T_{tran})$ is a convolution integral of Gaussian and Lorentzian lineshape contributions. Collisional quenching of the excited state is negligible in low pressure conditions, and therefore the fluorescence efficiency has been taken to be unity in Eq. (2).

Line broadening mechanisms cause contributions from closely spaced transitions to overlap. Pressure (Lorentz) broadening due to I_2–N_2 collisions is negligible at the low pressures encountered in this study. The observed broadening is almost entirely Doppler broadening due to the random, translational thermal motion of the gas molecules. The measured fluorescence signal is the sum of fluorescence from all excited absorption lines, each of which contributes an amount given by Eq. (2). The net signal due to excitation at laser frequency ν from N_t excited transitions is $S_f(\nu) = \sum_i^{N_t} S_{f_i}(\nu)$.

Due to nuclear electric quadrupole coupling and magnetic spin-rotation interactions in the I_2 molecule, rotational-vibrational lines exhibit hyperfine splitting. The P13 and R15 rotational lines of the (43–0) vibrational band each have hyperfine structure consisting of 21 components[4, 5]. The frequencies of these 42 hyperfine components span 1.23 GHz and are interleaved, as shown in the lower part of figure 2. The heights of the vertical lines in the figure indicate relative strengths of individual components.

In I_2 vapor at room temperature (290–300 K) and low pressure, the P13 and R15 lines appear as a single blended line with a Gaussian-like profile, due to significant Doppler broadening. Below 50 K, the Doppler broadening is sufficiently

1st order nuclear electric quadrupole + magnetic spin-rotation interaction model of hyperfine splitting for blended P48(44-0), P103(49-0) and P13(43-0), R15(43-0) transitions

FIGURE 3. Computed P48,P103 (at left) and P13,R15 hyperfine lineshape up to stagnation temperature, plotted at very low constant pressure.
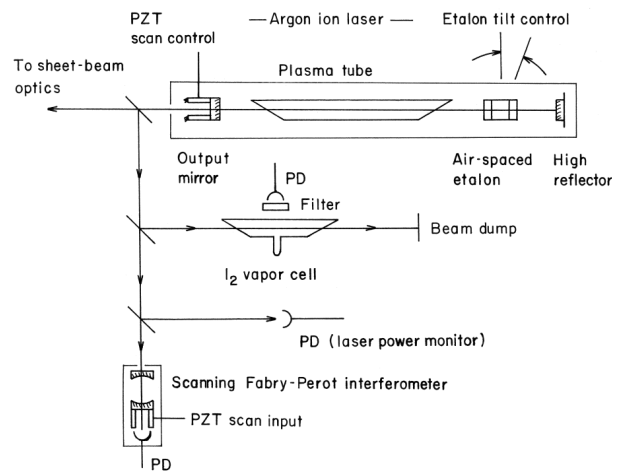
FIGURE 4. Laser set up.

low to reveal some of the underlying hyperfine structure. The computed (low pressure) P13,R15 lineshape $S_f(v)$ is plotted at several temperatures from 5 K to 25 K in figure 2. Because of the irregular, close spacing of the hyperfine components, only four distinct peaks are discernable at 25 K. At 10 to 15 K, seven distinct peaks can be distinguished. Further peaks appear in the lineshape at 5 K. Doppler broadening of the line shape is associated with the translational temperature.

Rotational temperature information is obtained by scanning an additional transition having a large rotational population at higher temperatures closer to ambient. For this purpose, the P48(49–0)/P103(44–0) transition is suitable. Figure 3 is a plot of both P13/R15 and P48/P103 blended transition lines. The Boltzmann population $f_{v''J''}$ of the ground vibrational-rotational state $v''J''$, which appears in equation 2 causes the intensity of the P48/P103 line to increase relative to the P13/R15 line at increasing rotational temperatures. Below about 30 K, the P48/P103 blended transition is relatively unpopulated and the uncertainty in measurement of rotational temperature using these lines increases significantly.

TEST FACILITY AND MEASUREMENT APPARATUS

Figure 4 is a schematic of the laser apparatus. A Spectra-Physics BeamLok 2080A-15 argon ion laser operating at 514 nm was used to excite I_2 fluorescence in the tests. A temperature-stabilized, air-spaced etalon mounted in the laser cavity eliminated all but one longitudinal mode of the laser.

To measure laser frequency, the beam was sampled by a heater-stabilized Fabry-Perot scanning interferometer (Spectra-Physics model 450) and passed through a room temperature I_2 cell. The locations of transmission fringes spaced 2 GHz apart in the interferometer scan output were monitored by a computer data acquisition system, and in conjunction with a cumulative fringe count, provided a relative frequency measurement during the tests. Fluorescence in the I_2 cell was measured with a photodetector to provide an absolute frequency reference.

The laser frequency was controlled in the following manner. The active longitudinal mode of the laser was selected by motorized adjustment of the etalon tilt angle, which shifts the frequency of the etalon loss curve minimum. The longitudinal modes were spaced 84 MHz apart. Finer frequency control of the laser was achieved by varying the laser cavity length. The laser output mirror could be moved up to 1.5 μm by applying a voltage to a piezoelectric translator. The resulting change in cavity length gave continuous fine frequency control over a few hundred MHz. The full range of the laser gain profile (about 10 GHz) was scanned in frequency increments down to 20 MHz by a combination of fine cavity length adjustments and "hopping" between longitudinal modes.

The laser beam was expanded 34× by a cylindrical lens, collimated, and focused into a thin, wide sheet which was cropped to a width of about 75 mm and passed through a window in the wind tunnel to excite fluorescence in a plane cutting through the flow.

A highly underexpanded free jet was produced by the expansion of I_2-seeded N_2 gas across a circular orifice of
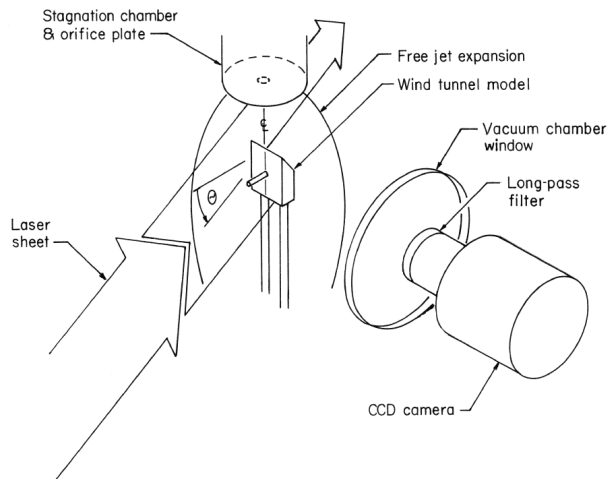
FIGURE 5. Experimental set-up for LIF imaging of the flow over the model in the low density wind tunnel.
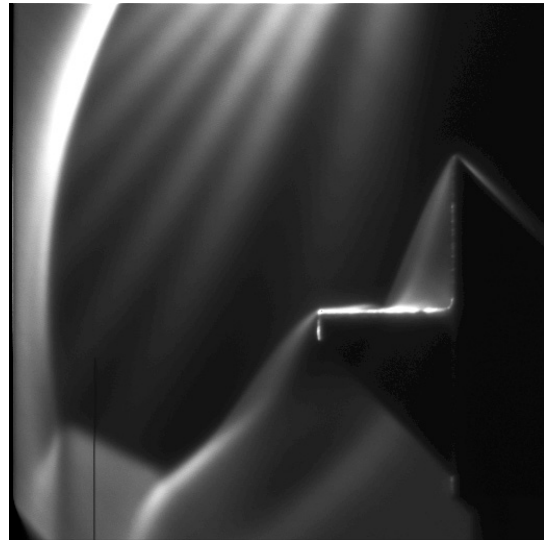
FIGURE 6. I_2 PLIF image of hypersonic flow over flat plate with protuding cylinder. Laser incidence $\theta = -45°$.

diameter $D = 2$ mm in a thin diaphragm into a continuously pumped vacuum chamber. Flow stagnation properties were measured in a settling chamber immediately upstream of the orifice. Gas issuing from the sonic condition at the orifice expands radially into a source-like hypersonic flow, forming a barrel-shaped shock wave that terminates at a curved normal shock known as the Mach disk. The hypersonic core of the free jet serves as the wind tunnel test section.

Figure 5 is a schematic of the PLIF test set-up. The test flow is produced by introducing a model inside the free jet core, upstream of the Mach disk location in the undisturbed free jet. The model consists of a 30 mm long flat plate which has a 2.38 mm diameter circular rod projecting perpendicular to its surface midway along its length. The model was constructed of aluminum plate and stainless steel rod and was painted flat black to minimize the amount of reflected and scattered laser light, since the laser sheet is incident on the model during the tests.

The flat surface of the model was centered along the symmetry axis of the undisturbed free jet, at zero incidence. The leading edge of the model was located approximately 41 mm (20.5 D) downstream of the orifice, where the effective freestream Mach number at the center of the leading edge, $M_{LE} \approx 11.9$, based on the correlation of Ashkenas and Sherman [6].

Images were taken with a Photometrics CH210 liquid nitrogen-cooled camera system using a PM512 CCD having a 516×516 array of 20 μm square pixels. This system allows acquisition of low noise, highly linear, 14-bit images under low light conditions. An 85 mm f/1.4 Nikon lens was employed with a 1.4$\times$ teleconverter, an 8 mm extension ring (to reduce the minimum focusing distance), and a 570 nm long-pass Schott glass filter to block scattered laser light. The camera was placed with a subject-to-image plane distance of about 76 cm, resulting in a spatial resolution of 11 pixels/mm. Due to an exposure time of 24 sec. for each image, only time-averaged fluorescence is recorded. The free-running laser jitters over an optical frequency bandwidth of at least 15 MHz, at temporal frequencies between 10–500 Hz, which causes it to be averaged over a single exposure. This frequency jitter produces undesirable instrumental broadening in the absorption spectra.

MEASUREMENTS

Measurements were taken in the symmetry plane of the model, which passes through the cylinder centerline, normal to the plate. Figure 6 is a narrowband I_2 PLIF image of flow over the plate-cylinder model in the wind tunnel. Light areas in the image are fluorescence patterns which arise due to the local flow conditions. The laser propagation direction, from left to right and downward at 45°, is indicated by the dark triangular region blocked by cylinder.

The least-squares curve fits minimized chi-squared for $T_{\rm rot}$ constrained from 6 K to 328 K in 10% increments and $T_{\rm tran}/T_{\rm rot}$ constrained from 1 to 1.95 in 10% increments. Figures 7 and 8 are contour plots of measured translational
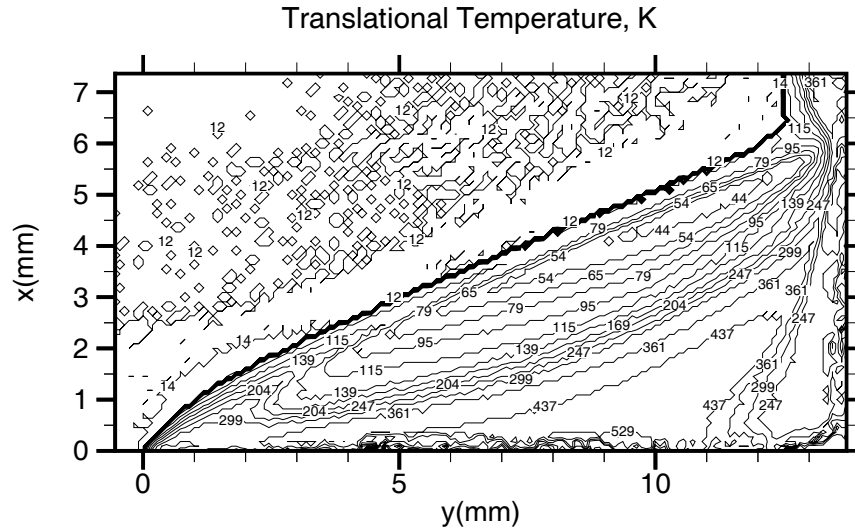
Translational Temperature, K

FIGURE 7. Contours of measured I_2 translational temperature on the plate, ahead of the cylinder.
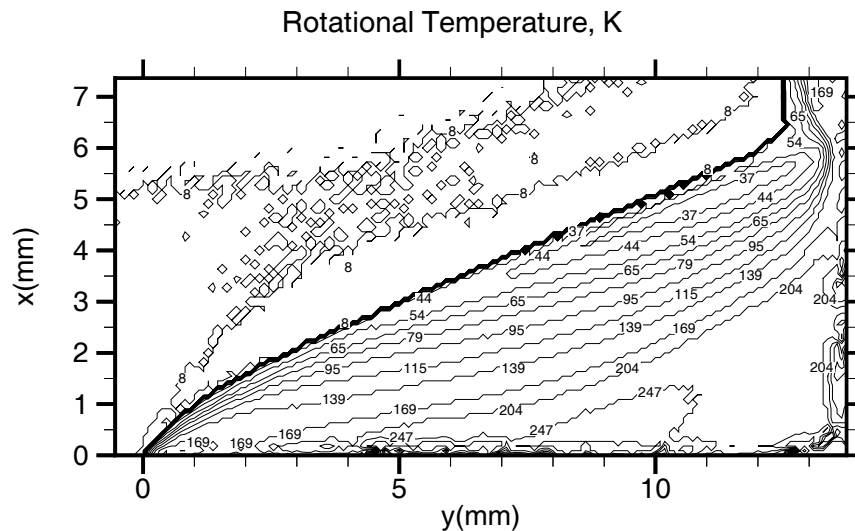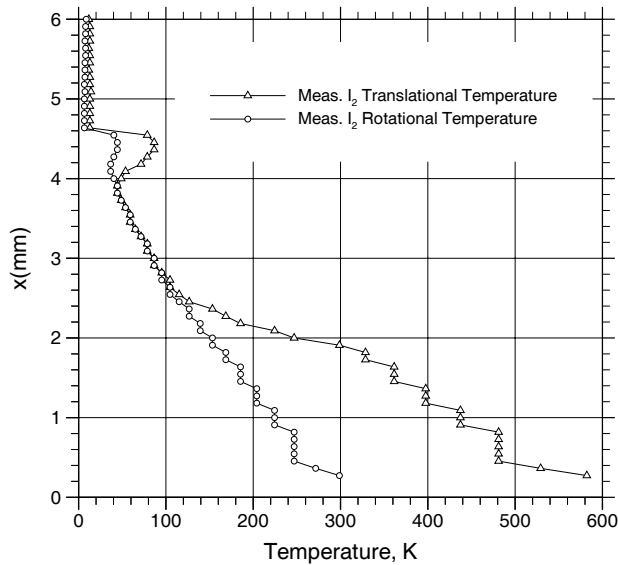
Rotational Temperature, K

FIGURE 8. Contours of measured I_2 rotational temperature on the plate, ahead of the cylinder.

and rotational temperature on the plate ahead of the cylinder. The surface of the plate is along $x = 0$, with the plate leading edge at $y = 0$ and the cylinder leading edge at $y = 13.8$ mm. The oblique shock develops an angle of about $23°$ with respect to the plate.

   The contour plots indicate that the translational and rotational temperature come to near equilibrium just upstream of the cylinder at about $y = 12$ mm, as the flow has been slowed to near stagnation.

   Profiles of the measured I_2 rotational and translational temperature at the location $y = 8.7$ mm on the plate are plotted in figure 9. The low temperature gas is heated as it flows over the room-temperature flat plate.

   The I_2 molecule is 9 times as massive as N_2, and this accounts for the large degree of nonequilibrium exhibited in the boundary layer. Due to its larger mass, I_2 has proportionally more translational kinetic energy at a given speed. When the N_2 carrier gas is slowed down, the I_2 molecules that are slowed must shed a greater amount of translational energy by collisions than the N_2 molecules to approach equilibrium. In the boundary layer, the random translational motion of the I_2 molecules in the y-direction is increased considerably by collisions with N_2 as the mean speed of the I_2 is reduced.

FIGURE 9. Profiles of measured rotational and translational temperature of I_2 on the plate at $y = 8.7$ mm.
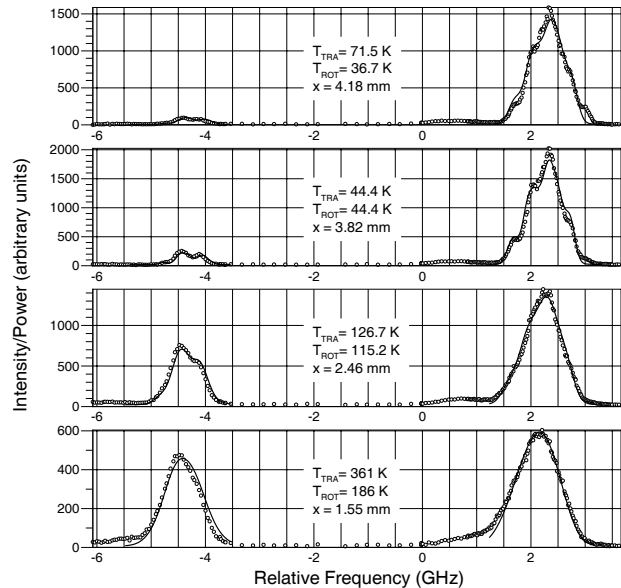
FIGURE 10. Measured I_2 LIF spectra and curve fits at selected points in the profile at $y = 8.7$ mm.

The same explanation applies to the I_2 as it flows through the oblique shock wave. The active translational mode across the oblique shock is normal to the shock wave. The direction of that mode is within about 22° of the direction of laser propagation, and so the measurement was sensitive to the active translational mode in that shock. The translational temperature overshoots the rotational temperature in the shock front and then relaxes into a near-equilibrium representing the theoretical post-shock condition.

The direction of laser propagation is significant in the measurement of translational temperature, which is related by a scalar (via the ideal gas law) to the pressure tensor. In nonequilibrium, the principal values of the pressure tensor may differ significantly. The translational temperature measurements presented here should be understood to indicate the kinetic temperature associated with random thermal motion in the direction of laser propagation, and not an overall translational temperature.

Examples of measured I_2 LIF spectra and the curvefits to the fluorescence model are plotted in figure 10.

ACKNOWLEDGMENTS

REFERENCES

1. D. E. Cecil, Ph.D. dissertation, University of Virginia, expected 2011.
2. Barry Edney, "Anomalous Heat Transfer and Pressure Distributions on Blunt Bodies at Hypersonic Speeds in the Presence of an Impinging Shock", FFA Report 115, The Aeronautical Research Institute of Sweden, Stockholm 1968.
3. A. C. Eckbreth, *Laser Diagnostics for Combustion Temperature and Species*, Taylor and Francis Books, New York, 1996.
4. M. D. Levenson and A. L. Schawlow, "Hyperfine Interactions in Molecular Iodine," *Phys. Rev. A* **6** 1, pp. 10–20 (1972).
5. D. J. Ruben, S. G. Kukolich, L. A. Hackel, D. G. Youmans, and S. Ezekiel, "Laser-Molecular Beam Measurement of Hyperfine Structure in the I_2 Spectrum," *Chem. Phys. Lett.* **22** 2, pp. 326–330 (1973).
6. H. Ashkenas, and F. S. Sherman, "The Structure and Utilization of Supersonic Free Jets in Low Density Wind Tunnels" in *Advances in Applied Mechanics, Supplement 3, Vol. 2*, Academic Press, New York, 1966.